PROTEIN DYNAMICS

RNA polymerase motions during promoter melting

Andrey Feklistov,[1]* Brian Bae,[1] Jesse Hauver,[1] Agnieszka Lass-Napiorkowska,[2] Markus Kalesse,[3] Florian Glaus,[4] Karl-Heinz Altmann,[4] Tomasz Heyduk,[2] Robert Landick,[5,6] Seth A. Darst[1]

All cellular RNA polymerases (RNAPs), from those of bacteria to those of man, possess a clamp that can open and close, and it has been assumed that the open RNAP separates promoter DNA strands and then closes to establish a tight grip on the DNA template. Here, we resolve successive motions of the initiating bacterial RNAP by studying real-time signatures of fluorescent reporters placed on RNAP and DNA in the presence of ligands locking the clamp in distinct conformations. We report evidence for an unexpected and obligatory step early in the initiation involving a transient clamp closure as a prerequisite for DNA melting. We also present a 2.6-angstrom crystal structure of a late-initiation intermediate harboring a rotationally unconstrained downstream DNA duplex within the open RNAP active site cleft. Our findings explain how RNAP thermal motions control the promoter search and drive DNA melting in the absence of external energy sources.

Bacterial RNA polymerase (RNAP) locates promoter elements in the genome, captures conserved bases of the nontemplate strand (nt-strand) –10 element DNA in complementary pockets on its surface, and loads the template strand (t-strand) into a narrow active site cleft to program RNA synthesis (Fig. 1A) (*1*–*4*). The width of the cleft is defined by an ~20-Å swinging motion of the RNAP clamp, a conserved structural module of all multisubunit RNAPs (*5*–*7*). Structural and solution studies have suggested that DNA is loaded and melted in the open cleft, which later closes for processive transcription (*5*, *8*, *9*). The dramatic conformational changes in both RNAP and DNA during promoter melting are accomplished without any external energy input, such as adenosine triphosphate (ATP) hydrolysis (*1*). To study RNAP dynamics during initiation steps, we biased its clamp in either open (oRNAP) or closed (cRNAP) conformations by use of a toolbox of well-characterized ligands (Fig. 1B and fig. S1) (*9*, *10*) and then followed promoter melting in real time with two different fluorescence assays that report on the early (*2*) and late (*11*) stages of melting, respectively.

First, we determined the state of the clamp during recognition of the –10 promoter element when RNAP extrudes the conserved A_{-11} and T_{-7} bases out of the double-stranded DNA (dsDNA) and into complementary pockets of the promoter-specificity σ-subunit (*2*). Recognition of the flipped bases nucleates strand separation and induces an ~90° bend in promoter DNA, positioning the downstream duplex across the cleft for further unwinding (Fig. 1A) (*1*). This nucleating step can be monitored by using the RNAP beacon assay (I), in which A_{-11} capture specifically enhances the fluorescence intensity of a probe covalently linked to σ near the A_{-11} binding pocket (Fig. 1C) (*2*, *12*). To focus on –10 element recognition, we studied how RNAP binds a dsDNA construct devoid of all promoter elements except for the –10 hexamer at its downstream end (–10 dsDNA) (table S1). With the RNAP beacon assay, such a construct produced a slow fluorescence rise (Fig. 1C), indicative of specific –10 recognition, because DNA of similar length without a –10 sequence gave no signal (fig. S2, A and B). cRNAP, generated by preincubation of RNAP with phage T4 gp2 protein (*9*, *13*), produced a stronger signal that saturated ~5 times faster, whereas oRNAP, formed with lipiarmycin (Lpm) (*10*), gave a weak signal resembling the addition of nonpromoter DNA (Fig. 1, C and D, and fig. S2, A and C). Rate enhancements nearly identical to that seen with gp2 were observed with myxopyronin (Myx) and ripostatin (Rip), which form cRNAP via a different mechanism (Fig. 1D and figs. S1 and S2, A and B) (*9*). Because the clamp modulators used in our experiments all bind at least 60 Å away from the –10 recognition site (fig. S1 and supplementary text), we rule out direct effects of their binding and conclude that only cRNAP is able to specifically recognize the –10 element out of the dsDNA.

To mimic the promoter recognition process in which RNAP locates the –10 element directed by interactions with upstream promoter elements, we added a consensus –35 hexamer to the DNA construct (–35/–10 dsDNA) (table S1) and observed that –10 recognition in this context also requires cRNAP (fig. S3). Because the RNAP/Lpm complex binds to upstream promoter regions (*14*, *15*) but is unable to recognize the –10 element, we propose that in the open form, which is predominant in solution (*9*), RNAP rapidly surveys the genome for upstream promoter elements, whereas transient clamp closure allows readout of the conserved nt-strand bases and nucleation of melting. Thermal fluctuations between the two RNAP forms with overlapping sequence specificities therefore optimize the promoter search in the presence of the overwhelming excess of nontarget DNA. The mechanism of promoter location involving large (~20 Å) clamp motions is reminiscent of a theoretical "search-and-fold" scheme proposed by Mirny and colleagues (*16*) to explain fast target location by a DNA binding protein, which so far has only been borne out for small proteins fine-tuning DNA recognition through subtle conformational changes (*17*, *18*).

To rule out assay-specific artifacts and to test our conclusions on a full-length native promoter, we used a different real-time fluorescence assay (II) reporting on late steps of promoter melting (*11*). We attached a Cy3 probe to the nt-strand +2 position of the extensively characterized λ P_R promoter (Fig. 2A and table S1). Changes in the local environment of the dye due to RNAP-induced promoter melting result in a twofold increase in fluorescence intensity, faithfully reflecting the multistep kinetics of λ P_R melting observed with chemical and enzymatic probing (*1*, *3*, *11*, *19*).

To gain kinetic insight into the melting step, we constructed a modified version of Cy3-λ P_R in which the base opposite A_{-11} was removed (Fig. 2A) in order to lower early kinetic barriers for melting nucleation by facilitating A_{-11} base flipping and DNA bending that accompany initial melting (*1*). In accord with our reasoning, upon addition of a saturating amount of RNAP, -11_tAb λ P_R displayed approximately threefold faster melting kinetics (Fig. 2B), suggesting that nucleation of melting is the rate-determining step. Next, we monitored promoter melting with both wild-type (WT) and -11_tAb λ P_R in the presence of clamp modulators. Myx (generating cRNAP) only marginally stimulated the melting on both templates (Fig. 2, C and D, and supplementary text). Lpm (oRNAP) completely prevented the melting on WT λ P_R because, as seen with the RNAP beacon assay (Fig. 1, C and D), oRNAP is unable to nucleate melting, which blocks all subsequent steps in the pathway. Remarkably, on -11_tAb λ P_R, the melting reaction was able to proceed slowly despite the presence of Lpm (Fig. 2D). Similar results were obtained when a mismatched base was placed opposite A_{-11} (fig. S4). Thus, –11 base-pair perturbations obviate the requirement for cRNAP, confirming that transient clamp closure nucleates melting.

As melting propagates downstream of the –10 element, the emerging single strands of DNA enter the RNAP active site cleft, which for steric reasons requires an open clamp (Fig. 1B) (*8*). To gain insight into this step, we determined a 2.6-Å-resolution crystal structure of oRNAP complexed with a downstream-fork DNA fragment, which was designed to mimic promoter binding during late stages of melting and supported specific initiation

[1]The Rockefeller University, 1230 York Avenue, New York, NY 10065, USA. [2]Edward A. Doisy Department of Biochemistry and Molecular Biology, Saint Louis University School of Medicine, St. Louis, USA. [3]Helmholtz Centre for Infection Research, Inhoffenstraße 7, 38124 Brunswick, Germany. [4]ETH Zürich, Department of Chemistry and Applied Biosciences, Institute of Pharmaceutical Sciences, Vladimir-Prelog-Weg 1-5/10 8093 Zürich, Switzerland. [5]Department of Biochemistry, University of Wisconsin–Madison, Madison, WI 53706, USA. [6]Department of Bacteriology, University of Wisconsin–Madison, Madison, WI 53706, USA.
*Corresponding author. Email: afeklistov@rockefeller.edu

in transcription assays (Fig. 3A, fig. S5, and table S2). The structure reveals DNA residing within the oRNAP cleft with excellent electron density for the –10 element nt-strand bound to σ^{A}_{2} (2) followed by a partially disordered downstream region that was excluded from the refinement (Fig. 3B and table S2).

Fragmented electron density in the downstream portion of the cleft is consistent with at least 8 base pairs (bp) of dsDNA (remaining from the 16-bp duplex originally present in the construct), suggesting that the promoter fragment was partially melted during cocrystallization (Fig. 3A), and its captured position likely represents a late intermediate of DNA loading into the cleft (RP_{i2}). This conclusion is further supported by the fact that the angle orienting the observed dsDNA along the expected trajectory of downstream promoter DNA during melting places the dsDNA

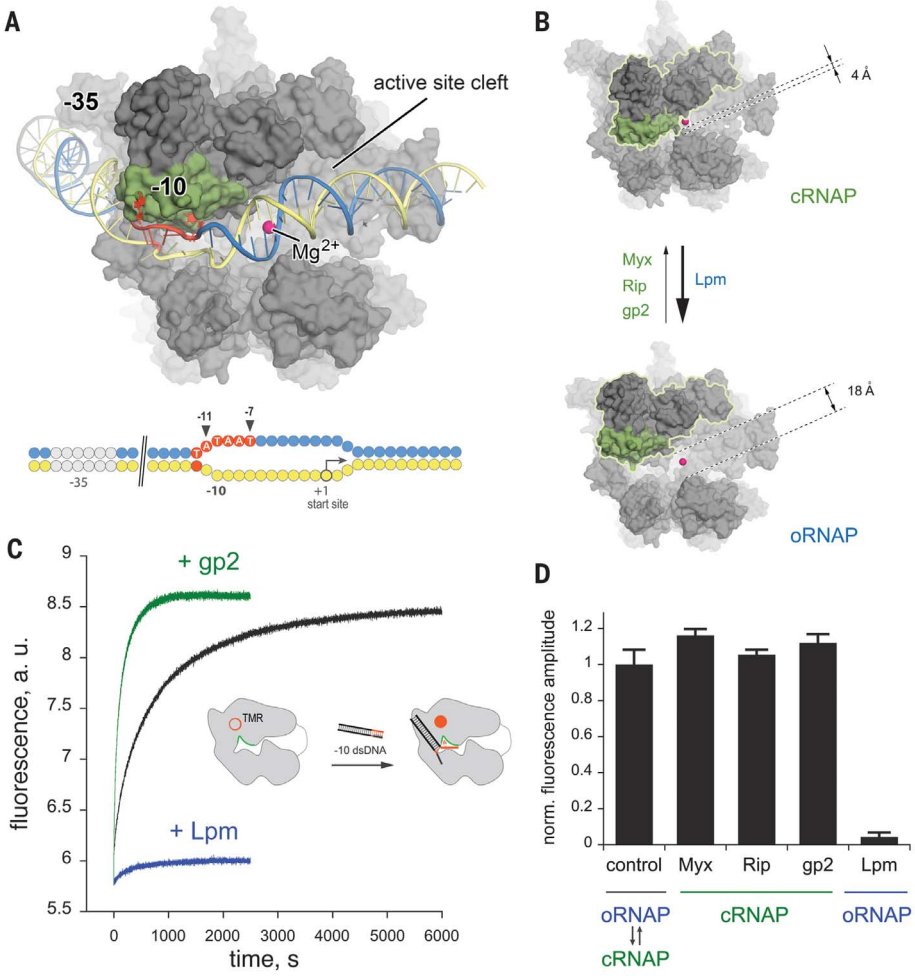

Fig. 1. Bacterial RNAP conformations and promoter recognition. (**A**) Model of a promoter melting intermediate with locally underwound –10 element DNA [based on PDB ID 1L9U (*26*, *27*)]. The –10 recognition surface of the σ-subunit is green, and the rest of the RNAP surface is gray. DNA strands are blue (nt) and yellow (t), with forked –10 element red, A_{-11} and T_{-7} bound in σ pockets, and –35 element in grey. (Bottom) schematics of fully melted bacterial promoter. Colors are as in (A), and conserved –11 and –7 positions of the nt-strand are highlighted. Numbers indicate positions before the start site (+1) (**B**) Ligands affecting the equilibrium between oRNAP and cRNAP conformations (*9*, *10*). The mobile β′ clamp and associated σ_2 domain regulating RNAP cleft width are highlighted. PDB IDs are 1L9U for oRNAP and 4XLN for cRNAP. (**C**) Time course of tetramethylrhodamine-labeled (red open circle and solid circle) RNAP (3 nM) fluorescence response to addition of 2 μM –10 element dsDNA. The black trace corresponds to unliganded RNAP, the green trace corresponds to cRNAP preincubated with gp2, and the blue trace corresponds to oRNAP preincubated with Lpm. (Inset) RNAP beacon assay I schematic. (**D**) Binding of –10 dsDNA to RNAP, cRNAP, or oRNAP measured with the RNAP beacon assay. SEM from at least three independent experiments are shown.

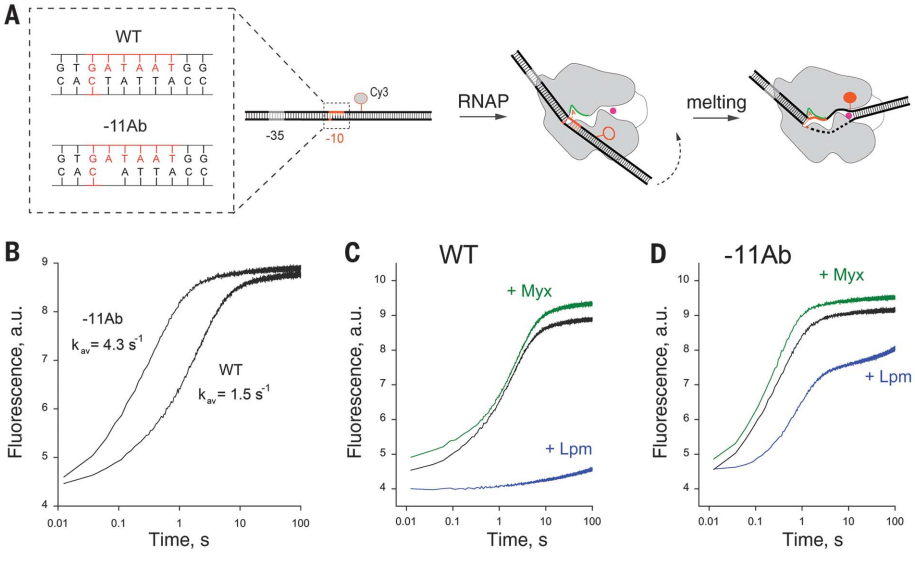

Fig. 2. Real-time kinetics of promoter melting and effects of cleft-locking ligands. (**A**) Fluorescence assay II. Cy3 (solid and open gray-filled red ovals) fluorescence enhancement reports on final steps of promoter melting (*11*). (Inset) –10 element sequence of WT and –11Ab λ P_R promoter variants. (**B**) Time course of Cy3-labeled WT and –11Ab promoters' response to addition of 100 nM RNAP. (**C** and **D**) WT and –11Ab promoter melting in assay II upon addition of 100 nM unliganded RNAP (black), cRNAP (preincubated with Myx; green) or oRNAP (preincubated with Lpm; blue).

in an intermediate position between the modeled largely unmelted DNA (RP_{i1}) and the downstream duplex of the fully melted promoter (RP_o) (Fig. 3D).

We observed an unusual disorder in the downstream dsDNA. A "ladder" of planar densities with ~3.4-Å spacing defined the base pair positions and the dsDNA helical axis (Fig. 3B). However, the base pair densities were "smeared" perpendicular to the helical axis and poorly resolved for 2.6-Å-resolution data (table S2). Moreover, density for the phosphate groups, typically the most prominent in nucleic acid electron density maps, was weak and poorly resolved (Fig. 3D). Taken together, these observations suggest that the downstream dsDNA in the crystallized complex retained a degree of rotational freedom along its helical axis. Several positively charged residues of the β′-subunit (R486, R1267, K1301, and

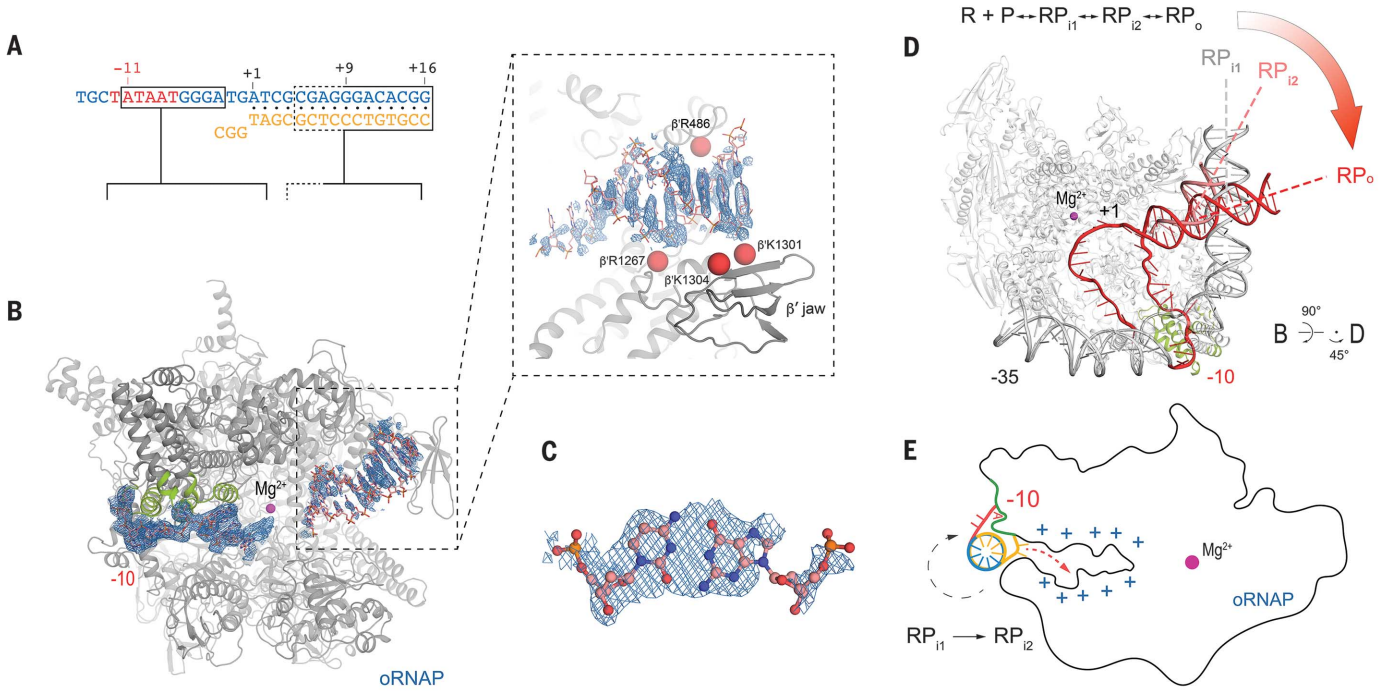

Fig. 3. Structure of oRNAP in complex with promoter fragment. (**A**) Promoter fragment used for cocrystallization, color coding, and numbering as in Fig. 1A. Boxed parts of the melted construct indicate DNA regions resolved in the structure, with dashed lines corresponding to poorly resolved density. (**B**) oRNAP shown in gray, with –10 element recognition surface in green. Blue mesh represents $2F_o–F_c$ map for the DNA displayed at 0.7σ contour level. (Single-letter abbreviations for the amino acid residues are K, Lys; R, Arg.) (**C**) Exemplary electron density, displayed as in (B), for base pair +14. (**D**) Downstream duplex trajectories in the intermediates of promoter melting [symbols on the lower right show how RNAP views in (B) and (D) relate]. Above the figure is the kinetic scheme of promoter melting. R, RNAP; P, promoter; RP_{i1}, modeled position of the intermediate preceding melting step; RP_{i2} (*26*), duplex DNA position observed in this work; RP_o, fully melted promoter DNA (*3*). (**E**) Spontaneous DNA unwinding during promoter melting. Schematic model of RP_{i1}–RP_{i2} transition is shown as the side view. Blue plus signs indicate positively charged surface of the RNAP active site channel (fig. S6).

Fig. 4. Schematics of RNAP structural transitions during promoter recognition and melting. Promoter DNA is shown in black lines, with –35 promoter element in gray and –10 element in red. Schematic of a sequence-dependent energy landscape of RNAP moving along the DNA in search of a promoter sequence is shown above, adopted from (*16*). Promoter search is optimized via interplay between oRNAP (blue; lower energy state, fast movement along DNA, scanning for upstream promoter elements, smooth binding energy landscape) and cRNAP (green; higher energy state, slower, precise DNA read-out, base flipping, rough binding energy landscape). –10 element recognition by cRNAP nucleates melting, followed by transition into oRNAP form, allowing DNA loading and unwinding in the cleft; the final closure seals the promoter complex.

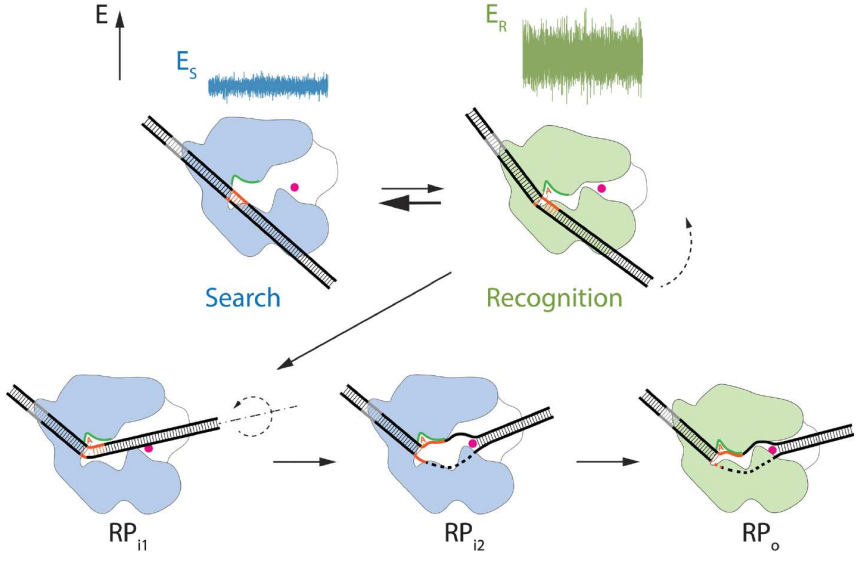

K1304) were located within electrostatic interaction distance from the expected phosphate positions of the duplex (Fig. 3B). Within 15 Å of the modeled DNA duplex in our structure are a total of 18 K and R residues, whose long aliphatic side chains with terminal positive charges possess high torsional freedom and are ideally suited to interact with the incoming downstream dsDNA yet allow the axial rotational freedom required for unwinding.

Strand separation nucleated by base flipping within the –10 element proceeds downstream via spontaneous base pair–breaking, with the emerging single strands of DNA pulled into the channel by the massive positive charge inside (Fig. 3E and fig. S5). The dimensions of the oRNAP cleft forbid the entrance of dsDNA, so it must stay above the cleft during early stages of melting (Fig. 3E). Only single strands of DNA (a total of 13 nucelotides long) can enter the oRNAP cleft, where they are progressively captured through electrostatic interactions until the fully melted bubble is generated and the downstream dsDNA reaches the binding site defined in this work. In support of this spontaneous, thermally driven mechanism is the steep temperature dependence of the promoter melting step (*1*) and the observation that melting does not proceed downstream of the –10 element if the cleft is widened by deletion of the β lobe domain (*20*).

Promoter melting by all multisubunit RNAPs, with the notable exception of eukaryotic RNA polymerase II (Pol II), is driven solely by binding free energy. Although melting by Pol II is generally thought to rely on the adenosine triphosphatase activity of transcription factor TFIIH, this requirement can be obviated in a number of cases [(*21*–*23*) and references therein]. Whereas the melting nucleation mechanisms may be specific for a given RNAP group, nearly identical cleft dimensions in bacterial, archaeal, and eukaryotic RNAPs (fig. S7 and supplementary text) (*24*) hint at a unified mechanism of melting propagation and t-strand loading into the cleft that may operate in all three domains of life.

Promoters display great variation in strength and sensitivity to regulatory factors that bind to RNAP, DNA, or both. Structural transitions of the transcriptional machinery delineated in this work (Fig. 4 and movie S1) can be viewed as checkpoints for gene regulation that contribute, along with factors modulating RNAP mobility (*25*), to the impressive dynamic range of gene expression.

REFERENCES AND NOTES

1. R. M. Saecker, M. T. Record Jr., P. L. Dehaseth, *J. Mol. Biol.* **412**, 754–771 (2011).
2. A. Feklistov, S. A. Darst, *Cell* **147**, 1257–1269 (2011).
3. B. Bae, A. Feklistov, A. Lass-Napiorkowska, R. Landick, S. A. Darst, *eLife* **4**, e08504 (2015).
4. Y. Zuo, T. A. Steitz, *Mol. Cell* **58**, 534–540 (2015).
5. P. Cramer, D. A. Bushnell, R. D. Kornberg, *Science* **292**, 1863–1876 (2001).
6. A. L. Gnatt, P. Cramer, J. Fu, D. A. Bushnell, R. D. Kornberg, *Science* **292**, 1876–1882 (2001).
7. S. A. Darst *et al*., *Proc. Natl. Acad. Sci. U.S.A.* **99**, 4296–4301 (2002).
8. D. G. Vassylyev *et al*., *Nature* **417**, 712–719 (2002).
9. A. Chakraborty *et al*., *Science* **337**, 591–595 (2012).
10. D. Wang, R. H. Ebright, Ensemble fluorescence resonance energy transfer analysis of RNA polymerase clamp conformation. Rutgers University Community Repository (2008).
11. J. Ko, T. Heyduk, *Biochem. J.* **463**, 135–144 (2014).
12. V. Mekler, O. Pavlova, K. Severinov, *J. Biol. Chem.* **286**, 270–279 (2011).
13. B. Bae *et al*., *Proc. Natl. Acad. Sci. U.S.A.* **110**, 19772–19777 (2013).
14. A. Tupin, M. Gualtieri, J.-P. Leonetti, K. Brodolin, *EMBO J.* **29**, 2527–2537 (2010).
15. Z. Morichaud, L. Chaloin, K. Brodolin, *J. Mol. Biol.* **428**, 463–476 (2016).
16. M. Slutsky, L. A. Mirny, *Biophys. J.* **87**, 4021–4035 (2004).
17. C. G. Kalodimos *et al*., *Science* **305**, 386–389 (2004).
18. C. Yi *et al*., *Nat. Struct. Mol. Biol.* **19**, 671–676 (2012).
19. J. Rammohan, A. Ruiz Manzano, A. L. Garner, C. L. Stallings, E. A. Galburt, *Nucleic Acids Res.* **43**, 3272–3285 (2015).
20. K. Severinov, S. A. Darst, *Proc. Natl. Acad. Sci. U.S.A.* **94**, 13481–13486 (1997).
21. Y. C. Lin, W. S. Choi, J. D. Gralla, *Nat. Struct. Mol. Biol.* **12**, 603–607 (2005).
22. C. Plaschka *et al*., *Nature* **533**, 353–358 (2016).
23. M. J. Bick, S. Malik, A. Mustaev, S. A. Darst, *PLOS ONE* **10**, e0119007 (2015).
24. F. Werner, D. Grohmann, *Nat. Rev. Microbiol.* **9**, 85–98 (2011).
25. S. Schulz *et al*., *Proc. Natl. Acad. Sci. U.S.A.* **113**, E1816–E1825 (2016).
26. K. S. Murakami, S. Masuda, S. A. Darst, *Science* **296**, 1280–1284 (2002).
27. C. A. Davis, C. A. Bingman, R. Landick, M. T. Record Jr., R. M. Saecker, *Proc. Natl. Acad. Sci. U.S.A.* **104**, 7833–7838 (2007).

ACKNOWLEDGMENTS

We thank L. Mirny, T. Record, T. Strick, D. Oren, and V. Mekler for helpful discussions and A. Kapanidis and R. Ebright for sharing and discussing unpublished data. This work was based in part on research conducted at the Advanced Photon Source (APS) Northeastern Collaborative Access Team beamlines funded by the National Institute of General Medical Sciences from NIH (P41 GM103403). The APS is a U.S. Department of Energy (DOE) Office of Science User Facility operated for the DOE Office of Science by Argonne National Laboratory under contract DE-AC02-06CH11357. The use of The Rockefeller University Structural Biology Resource Center was made possible by NIH/National Center for Research Resources grant 1S10RR027037. This work was supported by NIH grants R01 GM38660 to R.L. and R35 GM118130 to S.A.D. and FP7 grant 260872 to K.-H. A. The x-ray crystallographic coordinates and structure factors for oRNAP complexed with downstream promoter fragment is available at the Protein Data Bank with PDB ID 5TJG. A.F. conceived and oversaw the project, designed and performed kinetic experiments, analyzed kinetic and structural data, and wrote the paper with input from S.A.D and R.L. B.B. performed crystallization and structure determination with the help of S.A.D. J.H., A.L.-N., T.H., M.K., F.G., and K.-H.A. contributed new materials and reagents. S.A.D. procured funding for the project.

SUPPLEMENTARY MATERIALS

www.sciencemag.org/content/356/6340/863/suppl/DC1
Materials and Methods
Supplementary Text
Figs. S1 to S8
Tables S1 and S2
References (*28*–*46*)
Movie S1

16 January 2017; accepted 27 April 2017
10.1126/science.aam7858

RNA polymerase motions during promoter melting

Andrey Feklistov, Brian Bae, Jesse Hauver, Agnieszka Lass-Napiorkowska, Markus Kalesse, Florian Glaus, Karl-Heinz Altmann, Tomasz Heyduk, Robert Landick and Seth A. Darst

Science **356** (6340), 863-866.
DOI: 10.1126/science.aam7858

Trapping RNA polymerase in the act

The enzyme RNA polymerase (RNAP) finds promoter elements in the genome, separates (or "melts") the DNA strands, and transcribes the template DNA strand to give RNA. A mobile clamp in RNAP plays a key role in initiating transcription. Feklistov *et al.* locked the clamp of bacterial RNAP in distinct conformations by using small molecules. They then used fluorescent probes to monitor binding as the promoter DNA was separated. Unexpectedly, they found that the clamp transiently closed to nucleate DNA melting, opened to load single-stranded DNA into the active site, and then closed around the template strand to start transcription.

Science, this issue p. 863